Limnol. Oceanogr., 48(2), 2003, 777–786

Global estimates of enhanced solute transport in marine sediments

Christof Meile[1] *and Philippe Van Cappellen*
Department of Geochemistry, Faculty of Earth Sciences, Utrecht University, P.O. Box 80021, 3508 TA Utrecht, The Netherlands

Abstract

Pore-water solute transport processes acting in addition to molecular diffusion affect sediment biogeochemistry and benthic exchange fluxes. Given the relatively few direct measurements of enhanced transport intensities, there is a need for predictive relationships to calculate enhanced transport parameters from more readily available information. Here, enhanced diffusion coefficients and nonlocal mass transfer coefficients are obtained by comparing total and molecular diffusion fluxes of oxygen across the sediment–water interface. Semiempirical relationships for these coefficients are derived as functions of benthic oxygen uptake. According to these relationships, enhanced solute transport significantly affects sediment–water column exchanges in regions with large benthic oxygen fluxes, typically on the continental shelves. On a global scale, enhanced transport contributes approximately one third of the total benthic flux of oxygen and more than half of that of phosphate.

The sediment–water interface (SWI) constitutes a natural boundary in the oceans, across which the transport regimes of both solids and solutes change dramatically (Boudreau and Jørgensen 2001). For solutes, open-water turbulence gives way to molecular diffusion through the porous medium of the sediment. In the uppermost layers of marine sediments, however, biologically induced solute transport (bioirrigation) can exceed transport because of molecular diffusion (Archer and Devol 1992; Meile et al. 2001). Pore-water advection driven by pressure changes as a result of wave or tide action can also contribute significantly to solute transport fluxes in permeable sandy sediments in nearshore environments (Ziebis et al. 1996; Boudreau et al. 2001). Quantitative estimates of enhanced transport intensities are thus important in order to constrain benthic fluxes of dissolved nutrients or oxygen uptake at the seafloor.

Pore-water concentrations change significantly over depth scales of millimeters to decimeters and give rise to a typical vertical zonation of pore-water chemistry. The concentration gradients are the result of a multitude of different reaction and transport processes acting simultaneously, which complicates identification of the individual processes. Concentration profiles are therefore complemented by direct measurements of reaction and transport rates. Mathematical models that explicitly couple the reaction network to the transport processes further help with interpretation of the observational data. From model simulations, it is then possible to estimate reaction rates and fluxes that can be difficult to measure directly (Soetaert et al. 1996*b*; Van Cappellen and Wang 1996). However, because detailed information is generally required as input, such models tend to be applied only at sites where extensive data sets have been collected, although the underlying mathematical description is generally valid.

To overcome the scarcity of comprehensive, site-specific data sets, global relationships for various reaction and transport parameters have been developed. Such relationships estimate crucial model parameters from easily obtainable site characteristics. Although of an empirical nature, these relationships provide simple parameterizations that capture the combined effects of multiple factors and processes. Examples are global expressions relating particle mixing intensities plus depths of the bioturbated layer (Boudreau 1994, 1997), organic carbon degradation rates (Tromp et al. 1995), or fluxes of organic carbon and oxidants at the SWI (Middelburg et al. 1997) to water depth or sedimentation rate. Global relationships are particularly useful when averaging over relatively large spatial scales, as is the case in ocean models of coupled sediment and water column biogeochemistry (Soetaert et al. 2000; Archer et al. 2002).

Although enhanced solute exchange fluxes and associated transport intensities have been estimated at individual study sites (e.g., Smethie et al. 1981; Martin and Banta 1992; Meile et al. 2001), little has been presented in terms of a global synthesis. Jahnke (2001), however, reported a systematic trend in the relative importance of enhanced solute transport and molecular diffusion as a function of the total O_2 uptake by sediments. At low O_2 uptake fluxes, typical for the deep sea, total and diffusive O_2 fluxes across the SWI are of the same order of magnitude. At high O_2 uptake fluxes, as encountered in coastal environments, a large fraction of the total uptake of O_2 cannot be accounted for by molecular diffusion.

In this paper, we use measured O_2 fluxes across the SWI and pore-water O_2 gradients to derive global relationships for enhanced solute transport (i.e., transport not due to molecular diffusion) in marine surface sediments. Parameterizations are proposed for both diffusional and nonlocal transport descriptions. To illustrate the impact of enhanced solute transport, the global effects of enhanced transport on oxygen and phosphate fluxes at the seafloor are estimated.

Data and methods

To separate the contributions of molecular diffusion and enhanced transport to total solute fluxes across the SWI, we

[1] Corresponding author (meile@geo.uu.nl).

Acknowledgments

We thank F. Wenzhöfer for providing a data set in advance of publication and D. Archer for a compilation of his data. Insightful comments from two anonymous reviewers helped us improve the manuscript. This study was funded in part by the Netherlands Organisation for Scientific Research (NWO-Pionier Programme).

Table 1. Data description, sources and references.

O_2 flux across the SWI	
Coastal (Skagerrak and German Bight)	Forster et al. 1999
Continental shelf (Washington)	Archer and Devol 1992 Devol and Christensen 1993
Arctic (Svalbard)	Glud et al. 1998
Continental slope and rise (off central California)	Reimers et al. 1992
Deep sea (South Atlantic)	Glud et al. 1994
Deep sea (South Atlantic)	Wenzhöfer and Glud 2002
Deep sea (Northeast Pacific)	Cai and Reimers 1995
Bottom water O_2, temperature, and salinity	
Values from the water depth closest to the seafloor. Depth resolution ranges from 10 m near the sea surface to 500 m below 2,000 m, with a resolution of 1 by 1 degree between 60°N and 60°S	Levitus and Boyer 1994, available via http://ingrid.ldgo.columbia.edu
Topography	
ETOPO5 5×5 min U.S. Navy database sampled on a 1 by 1 degree grid between 60°N and 60°S to match the Levitus data set or taken for the entire globe to determine ocean floor area per water depth interval.	National Geophysical Data Center 1988, available via http://ingrid.ldgo.columbia.edu
PO_4 gradients	
Compilation of pore-water phosphate gradients at the SWI. See original references for details.	Colman and Holland 2000, available via http://www.ngdc.noaa.gov/mgg/sepm/archive

compare benthic fluxes obtained with different experimental approaches. Benthic fluxes due to molecular diffusion (F_{diff}) are estimated from vertical high-resolution pore-water concentration profiles (microprofiles) and molecular diffusion coefficients under in situ conditions (Reimers et al. 2001). Total solute fluxes (F_{tot}) (i.e., combining the contributions of molecular diffusion and enhanced transport) are estimated from in situ benthic chamber experiments. From the difference between F_{diff} and F_{tot}, enhanced transport parameters are deduced. Because of the relatively large available database, the analysis presented is based on O_2 microprofiles and O_2 benthic flux measurements.

Data set—Data sources for F_{diff} and F_{tot} are summarized in Table 1. Total exchange fluxes calculated from concentration changes measured in benthic chambers currently provide the most direct measurements of total solute fluxes across the SWI (Martin and Sayles 1994). To minimize the effect of spatial heterogeneity, only fluxes from the same station are compared. To avoid sampling artifacts (e.g., because of changing temperature and pressure during sample recovery; Glud et al. 1994), only benthic fluxes measured in situ are used here (Table 1). Solute fluxes can also vary significantly as a function of time: sediment O_2 uptake, for example, depends strongly on the delivery of organic matter and thence can exhibit seasonal variability (Sayles et al. 1994; Soetaert et al. 1996*a*). Therefore, we only compare F_{tot} and F_{diff} values determined at the same time.

The effect of small-scale topography on diffusive exchange fluxes calculated from one-dimensional concentration profiles (Jørgensen and Revsbech 1985; Røy et al. 2002) is expected to be negligible in the selected data set because gradients (where specified) were mainly measured across the diffusive boundary layer, just above the sediment surface. Thus, diffusive fluxes are used directly as reported in the studies listed in Table 1.

Empirical relationships—Comparison of measured total and diffusive benthic exchange fluxes directly quantifies the flux caused by processes other than molecular diffusion ($F_{xs} = F_{tot} - F_{diff}$). However, often only an estimate of the total O_2 sediment uptake is available. We therefore estimate molecular diffusion fluxes from total fluxes using an empirical fitting function. As constraints, we impose $F_{diff} \rightarrow F_{tot}$ when $F_{tot} \rightarrow 0$, whereas at all values of O_2 uptake, $F_{diff} \leq F_{tot}$. Here, we use the relationship in Eq. 1.

$$F_{diff} = \frac{500 \cdot F_{tot}}{646 + F_{tot}} \tag{1}$$

The numerical values are obtained from the best fit to the data set (Fig. 1; $r^2 = 0.79$), with both F_{diff} and F_{tot} in units of μmol cm^{-2} yr^{-1}. Other functions that give more weight to low O_2 fluxes were also tested. They result in similar predicted values of F_{diff} (Fig. 1).

In order to quantify the contribution of enhanced transport to O_2 exchange across the SWI on a global scale, total benthic O_2 exchange must also be estimated at sites without direct flux measurements. To this end, we use a relationship proposed by Wijsman (2000), which relates benthic O_2 uptake to water depth (Eq. 2).

$$F_{tot} = 23.22e^{-0.017z} + 3.78e^{-0.00047z} \tag{2}$$

z is water depth (m) and F_{tot} the benthic O_2 flux (mmol O_2 m^{-2} d^{-1}). Equation 2 is based on 528 flux estimates using a variety of measurement techniques ($r^2 = 0.71$), and predicted O_2 fluxes for water depths between 9,000 and 20 m range from 10 to 1,000 μmol cm^{-2} yr^{-1} (*see* chapt. 2 in Wijsman [2000] for a detailed discussion of the data and their analysis).

Representations of enhanced transport—Enhanced transport has been described as a diffusive (e.g., Goldhaber et al. 1977; Matisoff and Wang 1998), advective (e.g., Hammond et al. 1977; McCaffrey et al. 1980), or nonlocal process (e.g., Emerson et al. 1984; Meile et al. 2001). Here, we consider two commonly used representations of enhanced transport, based on diffusive and nonlocal parameterizations, whose applicability depend on the physical processes causing mixing, as well as frequency and length scale of mixing events (Boudreau 1986*a*, 1986*b*, Boudreau and Imboden 1987). The following equations relate the transport coefficients to the enhanced transport flux.

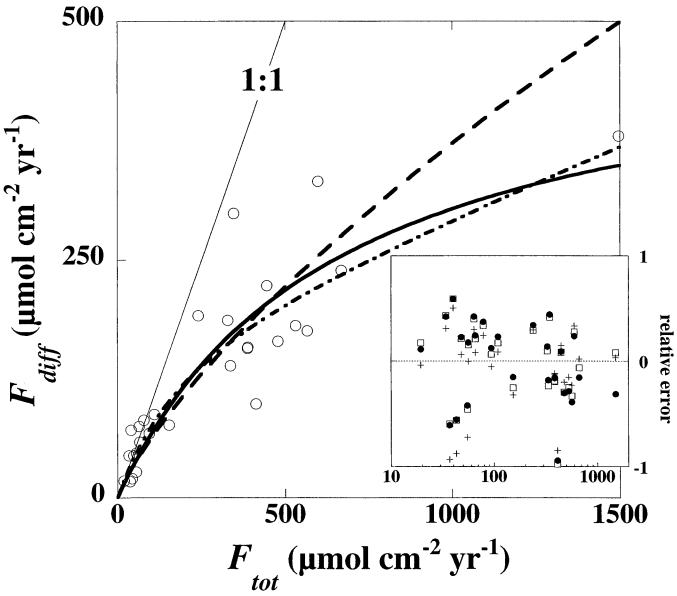

Fig. 1. Diffusive benthic O_2 fluxes derived from microprofiles versus total sediment–water O_2 exchange fluxes measured with benthic chambers. Circles represent the measured values and curved lines are three empirical fitting equations, all explaining ~80% of the measured values of F_{diff}. The thick line is Eq. 1 (squares in inset), the dashed line is a fit after log transformation of the fluxes—$\log(F_{diff} + 1) = [17.969 \log(F_{tot} + 1)]/[17.969 + \log(F_{tot} + 1)]$ (circles in inset)—and the dashed-dotted line (crosses in inset) is $\log(F_{diff}/F_{tot}) = (-0.839F_{tot})/(562.28 + F_{tot})$. The inset shows the relative residual errors, defined as $(F_{diff}^{calc} - F_{diff}^{meas})/F_{diff}^{meas}$, indicating that the relative error on F_{diff}, when estimated from F_{tot}, is ~30%.

$$\text{Diffusive:} \quad F_{xs} = -D_{enh}\phi \left.\frac{\partial C}{\partial x}\right|_{SWI} \tag{3}$$

$$\text{Nonlocal:} \quad F_{xs} = \int_{SWI}^{\infty} \alpha\phi(C_0 - C)\, dx \tag{4}$$

D_{enh} is the enhanced diffusion coefficient, α is the nonlocal transport coefficient (in units of inverse time), ϕ is porosity, C_0 is the solute concentration at the SWI, and x is the depth below the SWI.

Model assumptions—Equations 3 and 4 show that to determine the diffusive and nonlocal enhanced solute exchange coefficients, the concentration profile of the solute in the sediment must be known. Because we aim for global coverage of the seafloor (i.e, including sites where no measured O_2 profiles are available), pore-water O_2 concentrations must be calculated. In order to do so, we assume that porosity gradients and the effects of sedimentation and compaction are negligible. Additionally, the following assumptions underlie the model approach.

1. The O_2 concentration profile is at steady state. This is an appropriate assumption for the derivation of global ocean relationships, which do not account for transient, site-specific effects.
2. Benthic primary production is negligible, which excludes shallow clear-water sites from our analysis. The total benthic flux of oxygen is therefore related to the rate of O_2 consumption in the sediment, R, by

$$F_{tot} = \phi \int_{SWI}^{\infty} R\, dx \tag{5}$$

3. The rate of O_2 consumption is constant over the depth interval of O_2 penetration. Thus, R equals the input flux of O_2 into the oxic zone, divided by ϕ and the O_2 penetration depth, L. Quasi 0th-order rate profiles of net O_2 consumption have been reported in a number of studies (Berg et al. 1998; Glud et al. 1998) and are attributed to significant oxygenation of reduced inorganic species at the bottom of the aerobic surface layer. Nonetheless, other rate distributions have been reported and the effect of assuming a constant O_2 consumption rate with depth on enhanced solute transport parameters is therefore evaluated below.

Enhanced transport parameters—For a diffusive description of enhanced solute transport, the governing mass balance equation is

$$0 = (D_{sed} + D_{enh})\frac{\partial^2 C}{\partial x^2} - R \tag{6}$$

with $R = F_{tot}/\phi L$, where the enhanced diffusion coefficient is, for the sake of simplicity, assumed constant within the depth interval of O_2 penetration. The effective molecular diffusion coefficient, D_{sed}, is corrected for tortuosity using $D_{sed} \approx [D_{sol}(T, \text{sal})]/[1 - \ln(\phi^2)]$, where D_{sol} is the molecular diffusion coefficient in solution at in situ temperature (T) and salinity (sal) (Boudreau 1997). The conditions to be fulfilled by Eq. 6 are defined in Eq. 7.

$$C|_{x=0} = C_0, \qquad C|_{x=L} = 0, \qquad \left.\frac{\partial C}{\partial x}\right|_{x=L} = 0 \tag{7}$$

Equation 6 is solved for two endmember cases. In the first case, the O_2 penetration depth is assumed to be unaffected by enhanced O_2 delivery across the SWI (i.e., $L = L_{diff}$, where L_{diff} is the O_2 penetration depth when molecular diffusion is the only transport process [$D_{enh} = 0$]). In this case, enhanced transport results in an increase in the O_2 consumption rate, R, and Eq. 6 yields Eq. 8.

$$L = L_{diff} = \frac{2\phi C_0 D_{sed}}{F_{diff}} \tag{8}$$

In the second endmember case, R is assumed to reflect only the reactivity and abundance of reduced substances. Therefore, enhanced influx of O_2 into the sediment does not affect the magnitude of R, but only increases the depth of O_2 penetration (Eq. 9).

$$L = L_{diff}\frac{F_{tot}}{F_{diff}} = \frac{2\phi C_0 D_{sed}}{F_{diff}^2}F_{tot} \tag{9}$$

The two endmember estimates of L (Eqs. 8, 9) are compared to measured values in Fig. 2. Not unexpectedly, Eq. 8 tends to systematically underestimate the measured values, whereas Eq. 9 usually overestimates the depth of O_2 penetration. The arithmetic average of both equations, L, how-

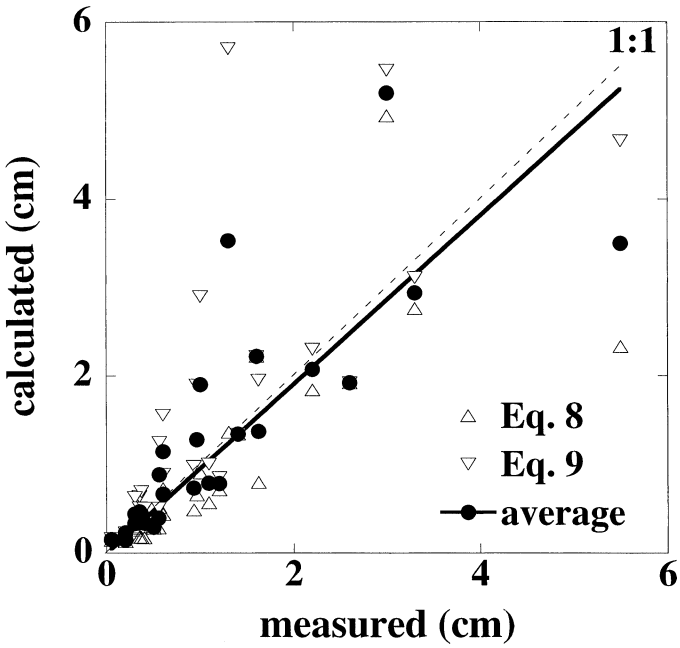

Fig. 2. Calculated and measured O_2 penetration depths. The thick line is the regression through the O_2 penetration depths obtained by averaging Eqs. 8 and 9 ($r^2 = 0.64$). The calculated O_2 penetration depths are based on measured values of F_{tot} and F_{diff} (*see* text for discussion).

ever, provides a remarkably robust predictor of the O_2 penetration depth (Fig. 2). Equation 6 is therefore solved for D_{enh} with L as the lower boundary depth. The relationship in Eq. 10 is obtained.

$$D_{enh} = \frac{1}{2}\left\{D_{sed}\left[\left(\frac{F_{tot}}{F_{diff}}\right)^2 - 1\right] + D_{sed}\left(\frac{F_{tot}}{F_{diff}} - 1\right)\right\} \quad (10)$$

The first term on the right-hand side results from $L = L_{diff}$ (Eq. 8), whereas the second term originates from assuming $L = L_{diff}(F_{tot}/F_{diff})$ (Eq. 9).

In contrast to the diffusive description, under nonlocal transport, O_2 can be delivered below the aerobic surface layer (Eq. 4), with O_2 being reduced along burrow walls in the otherwise anoxic sediment. Based on an analysis of α profiles from a variety of sites, Meile et al. (2001) concluded that only about 10–20% of the total benthic O_2 flux is delivered to the aerobic zone. Thus, for a quantification of enhanced solute mixing intensities, the entire α profile below the O_2 penetration depth must be known.

The driving force for enhanced transport is inherently connected to the sediment–water interface (e.g., through wave action or burrowing organisms); hence, decreasing transport coefficients with depth are often assumed (e.g., Martin and Banta 1992). Here, we consider a simple linear decrease of α from the SWI to x_{mix}, the solute mixing depth. The latter is assumed to coincide with the solid-phase mixing depth, which, based mainly on an analysis of ^{210}Pb profiles, has been proposed to be on the order of 10 cm across a wide range of marine sediments (Boudreau 1994). With a parabolic approximation of the O_2 profile between the SWI and L,

$$C(x) = C_0 - C_0\left(\frac{x^2 - 2xL + L^2}{L^2}\right)$$

and the average value of α in the oxic zone, $\bar{\alpha}$ (Eq. 11), is then obtained from Eq. 4.

$$\bar{\alpha} = \begin{cases} \dfrac{12x_{mix} - 6L}{L^2 - 4Lx_{mix} + 6x_{mix}^2}\dfrac{F_{xs}}{\phi C_0} & \text{for } L \le x_{mix} \\ \dfrac{6L}{x_{mix}(4L - x_{mix})}\dfrac{F_{xs}}{\phi C_0} & \text{for } L > x_{mix} \end{cases} \quad (11)$$

where x_{mix} is set to 10 cm. The assumption of a linear α depth distribution is evaluated below.

Uncertainty analysis—Several assumptions in the mathematical framework outlined above could affect the magnitude of the derived enhanced solute transport coefficients. Furthermore, uncertainties associated with the oxygen fluxes F_{tot} and F_{diff} also propagate into the estimated enhanced transport coefficients.

Rate profile: The rate of O_2 consumption might deviate from the proposed 0th-order kinetics. However, with the condition that the depth-integrated rate of consumption match the delivery of O_2 to the oxic layer, the O_2 profile and the O_2 penetration depth depend only weakly on the shape of the net rate profile. Relative to the constant rate scenario, a linearly increasing rate with depth ($R = kx$, for $0 \le x < L$, and $R = 0$, for $x \ge L$) results in an approximately 25% smaller L, whereas an exponentially decreasing rate profile ($R = ke^{-x/L}$ for $0 \le x < L$ and $R = 0$ for $x \ge L$) increases the O_2 penetration depth by about 20%. Thus, rate profiles deviating significantly from the proposed 0th-order kinetics produce O_2 penetration depths that lie within the range of the two endmembers used to estimate the O_2 penetration depth (Eqs. 8, 9). Furthermore, L and the concentration gradients at the SWI differ between the different rate descriptions in such a way that D_{enh} is unaffected by the selection of the rate profile when the conditions given by Eqs. 5 and 7 are fulfilled.

O_2 penetration depth: Although the estimate of $\bar{\alpha}$ is only weakly dependent on L, which is easily seen by substituting various values of L in Eq. 11, an erroneous estimate of L affects D_{enh}. Comparison of D_{enh} values calculated using $L = L_{diff}$ (Eq. 8) and $L = L_{diff}(F_{tot}/F_{diff})$ (Eq. 9) as lower and upper limits for L, and using Eq. 1 to predict F_{diff}, shows a $\pm 50\%$ variation of D_{enh} values around the best estimates obtained with Eq. 10.

Nonlocal mixing profile: In order to evaluate the effect of the shape of the α profile on the estimated average α value in the aerobic layer, Eq. 11 is compared to (1) an α profile constant down to x_{mix} and 0 below, (2) a constant α down to L and linearly decreasing below L to reach 0 at x_{mix}, and (3) an exponentially decreasing α profile with 95% of the mixing intensity taking place above x_{mix}. All α cases are based on a parabolic concentration profile and conservation of mass for O_2. The resulting $\bar{\alpha}$ values in the oxic zone are given by

$$\bar{\alpha} = \begin{cases} \dfrac{3L^2}{-x_{\text{lim}}^3 + 3x_{\text{lim}}^2 L + 3L^2 x_{\text{mix}} - 3L^2 x_{\text{lim}}} \times \dfrac{F_{\text{xs}}}{\phi C_0}: & \text{case (1)} \\ \dfrac{6(x_{\text{mix}} - L)}{-4L^2 - 8Lx_{\text{mix}} + 9x_{\text{mix}}^2 - 3x_{\text{lim}}^2 + 12Lx_{\text{lim}} - 6x_{\text{mix}}x_{\text{lim}}} \times \dfrac{F_{\text{xs}}}{\phi C_0}: & \text{case (2)} \\ \dfrac{p^2 L(e^{pL/x_{\text{mix}}} - 1)}{2x_{\text{mix}}^2(e^{pL/x_{\text{mix}}} - 1) - 2x_{\text{mix}}pL - p^2L^2e^p} \times \dfrac{F_{\text{xs}}}{\phi C_0}: & \text{case (3)} \end{cases} \tag{12}$$

for the three respective α profile shapes, with $x_{\text{lim}} = \min(x_{\text{mix}}, L)$ and $p = \ln(1 - 0.95)$. Although the calculated $\bar{\alpha}$ values differ significantly among the various scenarios, the relative difference in $\bar{\alpha}$ between the linear and the other profile shapes is <60%, and the linearly decreasing α profile gives $\bar{\alpha}$-values intermediate between the other scenarios.

Mixing depth: The mixing depth, x_{mix}, can vary from site to site, and mixing depths are not necessarily equal for solids and solutes, as transport processes can differ. Thus, the sensitivity of the average value of α in the oxic layer toward x_{mix} is evaluated. Ignoring covariances, the uncertainty (σ_P) associated with a parameter P can be expressed as

$$\sigma_P = \sqrt{\sum_i \left(\frac{\partial P}{\partial X_i}\right)^2 \sigma_{X_i}^2} \tag{13}$$

where σ_X is the uncertainty associated with the independent parameter X. Identifying P as $\bar{\alpha}$ (Eq. 11) and X as x_{mix}, the relative error in $\bar{\alpha}$ for $L < x_{\text{mix}}$ is equal to

$$\frac{2(L^2 - 6Lx_{\text{mix}} + 6x_{\text{mix}}^2)}{(L^2 - 4Lx_{\text{mix}} + 6x_{\text{mix}}^2)(2x_{\text{mix}} - L)}\sigma_{x_{\text{mix}}}$$

which yields a relative error in $\bar{\alpha}$ between 0.65 and 1.1 times the relative error in x_{mix}: $\sigma_{x_{\text{mix}}}/x_{\text{mix}}$. This can be significant at any individual study site, but it is rather small when considering global relationships.

O_2 fluxes: Although the general trend of F_{diff} vs. F_{tot} is captured by Eq. 1, the considerable uncertainties on predicted F_{diff} values (Fig. 1 inset) lead to significant uncertainties in the calculated transport parameters. Because some of the independent variables (X, Eq. 13), such as the molecular diffusion coefficient, C_0 or ϕ are either experimentally accessible, remain fairly constant, or both, the uncertainty in D_{enh} or $\bar{\alpha}$ (σ_P, Eq. 13) reflects mostly the uncertainty on the fluxes (F_{tot}, F_{diff}). Expressing F_{diff} as a function of F_{tot} (Eq. 1), an approximate measure for the uncertainties associated with the predicted enhanced transport parameters is obtained when substituting P in Eq. 13 by Eq. 10 and 11, respectively. This analysis indicates that, within the conceptual framework developed above, estimates of D_{enh} are more sensitive to errors in F_{tot} and F_{diff}, than estimates of $\bar{\alpha}$ (Fig. 3).

Figure 3 also shows that for both diffusive and nonlocal descriptions, the uncertainties of the predicted transport coefficients are in a reasonable range when the total sediment O_2 uptake is known (the relative error in the prediction of F_{diff} from F_{tot}, $|\sigma_{F_{\text{diff}}}/F_{\text{diff}}|$, is on the order of 30%, Fig. 1 inset). However, when F_{tot} is estimated from, say, water depth, the relative error in F_{tot} can easily be 50%, which increases the uncertainty of transport parameter estimates considerably. The predicted transport coefficients are more prone to error at low total O_2 uptake (Fig. 3), which typically corresponds to greater water depths and lower enhanced transport intensities.

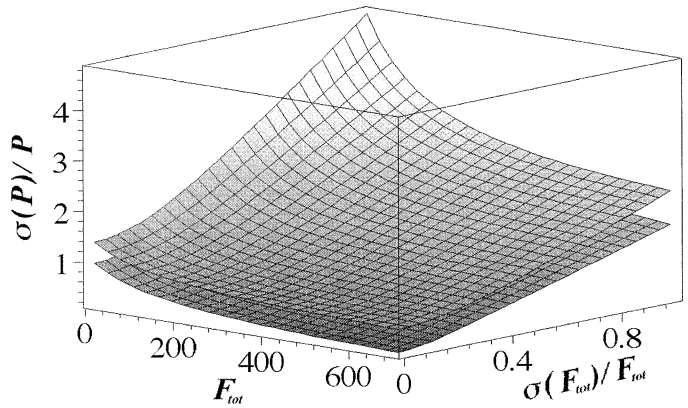

Fig. 3. Relative error on the enhanced transport coefficients as a function of F_{tot} (μmol cm^{-2} yr^{-1}) and the relative uncertainty on F_{tot}. The upper and lower surfaces correspond to enhanced diffusion and nonlocal transport, respectively. For the calculations, F_{diff} is estimated from F_{tot} by Eq. 1, $\sigma_{F_{\text{diff}}}/F_{\text{diff}}$ is set to 30% (Fig. 1), porosity is 0.8, D_{sed} is 200 cm^2 yr^{-1}, and the O_2 concentration in the overlying water is assumed to be 100 μM.

Results and discussion

Enhanced O_2 uptake at the seafloor—The global contribution of enhanced solute transport to benthic O_2 exchange fluxes is estimated using the relationship between F_{diff} and F_{tot} (Eq. 1). Benthic O_2 fluxes are calculated as a function of water depth (Eq. 2, water depths >20 m, the depth cutoff is chosen to exclude areas with a major contribution of benthic primary production). Total sediment O_2 uptake is then obtained through multiplication with the corresponding ocean floor surface areas, calculated from the ETOP bathymetric map on a 1° by 1° grid (Table 1). This analysis suggests that >40% of the total mass of O_2 is taken up by sediments located at water depths shallower than 300 m. A significant portion, about a third of the total O_2 uptake at the entire seafloor, is estimated to be due to enhanced transport. This fraction drops by ~10% when considering only water depths >100 m rather than 20 m.

Such a significant contribution of enhanced benthic O_2 uptake in continental margin environments implies a pronounced impact on the early diagenetic pathways of organic matter degradation. For example, enhanced supply of O_2 can substantially promote the reoxidation of reduced inorganic species, such as sulfide, thereby sustaining sulfate availability and high sulfate reduction rates (Ferdelman et al. 1999; Fossing et al. 2000; Koretsky et al. unpubl. data) and preventing methanogenesis.

Patterns in enhanced transport—To assess enhanced transport on a global scale, transport coefficients are calculated for the ocean between 60°N and 60°S on a 1° by 1° grid. This resolution is dictated by the availability of O_2, temperature, and salinity data (Levitus data set, Table 1), which are used to obtain C_0 and $D_{sed}(O_2)$ for each grid point. Porosity near the SWI is typically between 0.75 and 1, and for the global simulations is assumed to be 0.8. Enhanced transport coefficients are calculated from estimates of total O_2 solute exchange fluxes (Eq. 2, with water depth based on the ETOP map), estimating F_{diff} from F_{tot} (Fig. 1) and using Eqs. 10 and 11, respectively.

In addition to the transport coefficients obtained on the 1° by 1° grid, results from the individual study sites listed in Table 1, based on measured values of L, F_{tot}, F_{diff}, and C_0, are shown in Fig. 4. The two enhanced solute transport representations, D_{enh} and $\bar{\alpha}$, derived from the global ocean grid show similar patterns with depth or total benthic O_2 flux. As expected, enhanced transport coefficients are high relative to diffusive exchange at high total benthic O_2 fluxes, where F_{xs} becomes significant (Fig. 1). Model results suggest that at total O_2 fluxes smaller than ~100–150 μmol cm^{-2} yr^{-1}, which according to Eq. 2 roughly correspond to water depths >250–400 m, molecular diffusion is the dominant transport mechanism (Fig. 4A). Results from site-specific calculations show a somewhat larger range of F_{tot}, where coefficients of molecular diffusion and enhanced diffusion are of similar magnitude (about 50–250 μmol cm^{-2} yr^{-1}, Fig. 4A). The solid-phase mixing coefficient D_b, estimated from water depth (Middelburg et al. 1997), is systematically smaller than either the molecular or the enhanced diffusion coefficient (by an order of magnitude or more, not shown), indicating that solid-phase mixing has, globally, a minor effect on solute transport in marine sediments.

Generally, poorer agreement exists between the global grid and the site-specific estimates of enhanced transport coefficients at low benthic O_2 uptake fluxes (Fig. 4). This reflects the large (relative) uncertainties associated with estimates of enhanced transport coefficients at low F_{tot} (Fig. 3) and thus low F_{xs}. However under these conditions, characteristic for the deep sea, enhanced transport tends to play a minor role in benthic solute fluxes. At benthic uptake fluxes > 100 μmol cm^{-2} yr^{-1}, site-specific enhanced transport parameters show increasing trends with F_{tot}, similar to those observed for the global grid results.

Global relationships—When the benthic O_2 flux, F_{tot}, is known at a given site, enhanced transport coefficients can be calculated by combining an estimate of F_{diff} derived from F_{tot} (Fig. 1) with Eq. 10 (D_{enh}) or Eq. 11 ($\bar{\alpha}$). For sites where the benthic O_2 flux has not been measured, we recommend estimation of F_{tot}, for example, from the total organic carbon mineralization rate. In both cases, site-specific values of the other input parameters—$D_{sed}(O_2)$, ϕ, L, and C_0—should be used preferably.

When not all the necessary site-specific information is available, or when simple parameterizations are needed for use in biogeochemical models of the whole ocean, the empirical Eqs. 14–17 can be used. These equations are derived by fitting the entire set of transport coefficients calculated for the global ocean grid (Fig. 4).

$$D_{enh} = (7.6375 - 7.4465e^{-0.00089603F_{tot}(O_2)})D_{sed}(O_2) \quad (r^2 = 0.99) \tag{14}$$

$$\bar{\alpha} = (-73.071 + 71.912e^{-0.0013846F_{tot}(O_2)})C_0^{-1} \quad (r^2 = 0.99) \tag{15}$$

$$D_{enh} = 48{,}133 - 48{,}089e^{-0.000046764F_{tot}(O_2)} \quad (r^2 = 0.94) \tag{16}$$

$$\bar{\alpha} = -1{,}591.7 + 1{,}580.8e^{-0.00055127F_{tot}(O_2)} \quad (r^2 = 0.21) \tag{17}$$

The units are cm^2 yr^{-1} for D_{enh} and $D_{sed}(O_2)$, μmol cm^{-2} yr^{-1} for $F_{tot}(O_2)$, yr^{-1} for $\bar{\alpha}$, mM for the O_2 bottom water concentration, C_0; the r^2 values refer to the fit to the global grid rather than the site-specific results.

Comparison of the r^2 values reveals that $\bar{\alpha}$ cannot be predicted accurately from F_{tot} alone (Eq. 17); $\bar{\alpha}C_0$, however, strongly correlates with F_{tot} (Eq. 15). The globally predicted $\bar{\alpha}C_0$ values also agree well with the site-specific values (Fig. 4B). Use of the nonlocal transport description therefore requires knowledge of the O_2 bottom water concentration. For D_{enh}, only a moderate increase in r^2 is observed when variations in D_{sed} are taken into account. However, the good fit of Eq. 16 to the global grid parameter values partially reflects the correlation between bottom water temperature and water depth (*see* analysis of the Levitus data set in Tromp et al. [1995]) and that F_{tot} is estimated from water depth (Eq. 2). Therefore, we recommend the use of Eq. 14 when salinity and temperature (and possibly porosity) values are available to estimate D_{sed}.

Equations 15 and 14 or 16 allow one to predict enhanced transport coefficients from the benthic O_2 uptake flux. Alternatively, the parameters can be obtained from water depth, z, by substituting Eq. 2 into Eqs. 14–16. This increases the uncertainty on the parameter values, however, because of the propagation of errors associated with estimating F_{tot} from z (Fig. 3).

Comparison to other studies—The finding that enhanced transport is significant in nearshore and continental shelf environments is supported by studies at individual sites (e.g., Archer and Devol 1992), and enhanced diffusion coefficients in shallow North Sea sediments are several times higher than molecular diffusion coefficients (Vanderborght et al. 1977). The model prediction that enhanced solute mixing tends to be less important in deep-sea sediments also agrees with experimental studies (Reimers and Smith 1986). Our estimates of enhanced diffusion coefficients fall in the range reported in (Berg et al. 2001), where it was shown that solute mixing coefficients exceed solid-phase D_b values by a factor of 15–20 at a nearshore site. Our results thus support that enhanced solute diffusion coefficients cannot be adequately approximated by solid-phase mixing parameters.

Nonlocal transport coefficients agree well with results from independent modeling approaches. In shallow-water carbonate sediments of Dry Tortugas, Florida, both early dia-

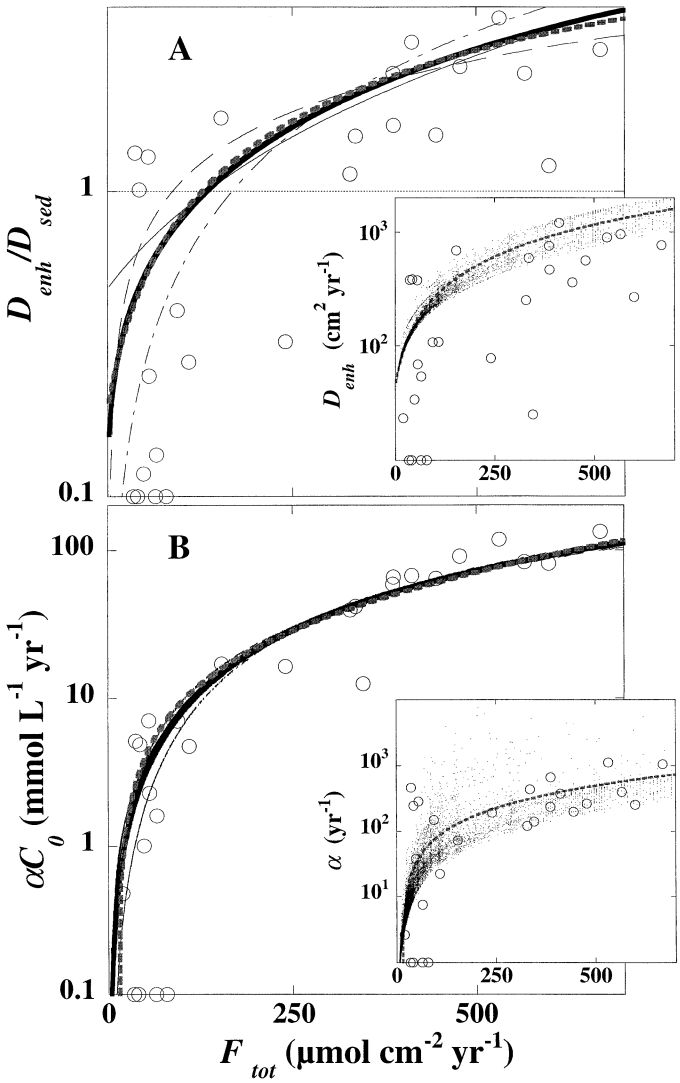

Fig. 4. Enhanced solute transport coefficients—(A) diffusional, (B) nonlocal—as a function of the total benthic O_2 uptake flux. Circles denote site-specific estimates (Table 1); dots are the coefficients estimated for the global grid. The thin lines in panels A and B correspond to the predicted parameter values using the three different empirical equations to estimate F_{diff} from F_{tot} (Fig. 1). The line patterns are the same as in Fig. 1. The thick lines in panels A and B correspond to the predicted parameter values using the arithmetic mean of the three empirical equations to estimate F_{diff}. The thick dashed lines represent the functions obtained by curve fitting the global grid estimates of Eqs. 14 (A), 16 (A inset), 15 (B), and 17 (B inset). For plotting purposes, when the measured F_{diff} exceeds F_{tot}, transport coefficients are set to the arbitrarily chosen minimum value of the *y*-axis.

genetic and stochastic modeling approaches give α values near the SWI between 3×10^{-6} (Furukawa et al. 2000) and $4–6 \times 10^{-6}$ s^{-1} (Koretsky et al. 2002). The $\bar{\alpha}$ value calculated here, 2.7×10^{-6} s^{-1}, is in excellent agreement with these studies (F_{tot} = 96 μmol cm^{-2} yr^{-1}, F_{diff} = 61 μmol cm^{-2} yr^{-1}, L = 0.26 cm, C_0 = 141 μM, ϕ = 0.58; data from Furukawa et al. [2000]). Predicted $\bar{\alpha}$ coefficients in the oxic zone of three sediments of the Skagerrak agree with the values in Wang and Van Cappellen (1996) to within 7–25%, if their modeled O_2 fluxes are used to calculate $\bar{\alpha}$. If Eq. 1 is applied to estimate F_{diff}, the values are still within 7–35% of each other ($4.1–9.4 \times 10^{-6}$ s^{-1} calculated here vs. $5.6–7.9 \times 10^{-6}$ s^{-1} used in Wang and Van Cappellen [1996], respectively). On the Washington shelf, $\bar{\alpha}$ values obtained based on total O_2 fluxes from Christensen et al. (1984) at two sites are 5.1×10^{-6} s^{-1} and 9.5×10^{-6} s^{-1}, respectively. This compares favorably to inverse modeling results based on radon and sulfate profiles, which lead to values of 3.7×10^{-6} s^{-1} and 6.2×10^{-6} s^{-1}, respectively (Meile et al. 2001).

Benthic phosphate fluxes—Colman and Holland (2000) have recently assessed the efflux of nutrient phosphate from marine sediments on a global scale. Based on 193 measured pore-water phosphate gradients (Table 1), they calculated benthic phosphate fluxes, taking into account molecular diffusion but assuming a negligible contribution from enhanced solute transport. Here, we examine the potential effect of enhanced transport on benthic regeneration of phosphate using the enhanced diffusion approach. The latter can be directly applied to the pore-water gradients compiled by Colman and Holland (2000).

For many of their sites, Colman and Holland (2000) provide organic carbon deposition and burial fluxes. We use the difference between these fluxes as a measure of the total organic carbon oxidation rate and, hence, of the total benthic O_2 uptake flux, $F_{tot}(O_2)$. For each site, the diffusion flux, $F_{diff}(O_2)$, is obtained from $F_{tot}(O_2)$ by taking the average of the three fitting functions shown in Fig. 1. A value of D_{enh} can then be calculated with Eq. 10. This value, together with the measured phosphate gradient, porosity, and molecular diffusion coefficient of phosphate given in Colman and Holland (2000), allows us to estimate the benthic flux of phosphate at the site.

In their global budget, Colman and Holland (2000) divided the ocean into two provinces—the Shelf–Slope and the Rise–Deep Sea—each characterized by an average sedimentation rate, ω. Following the same approach, we estimate the average benthic phosphate flux in each province from the empirical relationship between the benthic phosphate flux and ω obtained for the entire set of sites. The total flux of phosphate from the seafloor in each province is then estimated by multiplying the average flux by the corresponding surface area of the province (Fig. 5). A more detailed calculation, based on a greater number of water depth intervals derived from the ETOP map (Table 1) and using a global relationship between ω and water depth (Middelburg et al. 1997), results in essentially the same global benthic flux of phosphate (<5% difference).

The results in Fig. 5 indicate a large effect of enhanced transport on the flux of phosphate from the seafloor. This effect is particularly pronounced along the ocean margins, where enhanced transport dominates the benthic exchange of phosphate. Although the diffusion model might not be the most appropriate representation of enhanced transport of pore-water phosphate on a global scale, a preliminary analysis of pore-water profiles using the nonlocal model shows a similarly large contribution of enhanced transport on the benthic efflux of phosphate (results not shown). Thus, ig-

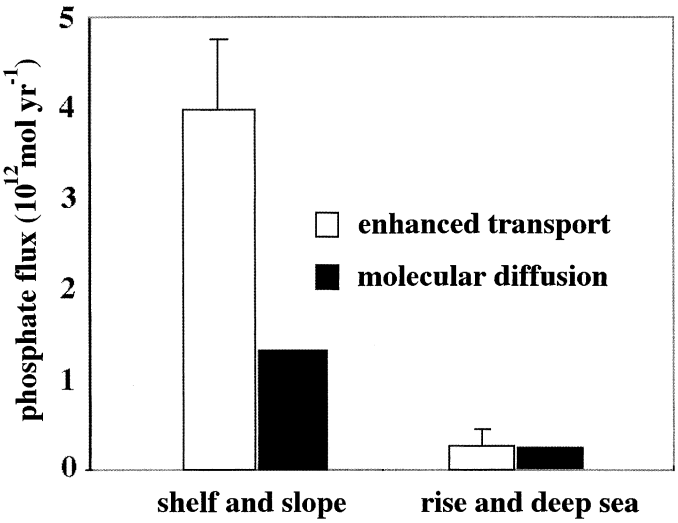

Fig. 5. Global benthic phosphate fluxes. The figure illustrates the large relative contribution of enhanced transport in continental margin sediments. Error bars give standard deviations originating from the different estimates of $F_{diff}(O_2)$ from $F_{tot}(O_2)$ (Fig. 1). Actual uncertainties on the absolute fluxes are significantly larger (*see*, in particular, fig. 2A in Colman and Holland 2000).

noring enhanced pore-water transport could introduce significant errors when estimating benthic fluxes of phosphate and, most likely, of other dissolved nutrients.

Synthesis and perspectives—The proposed global relationships for enhanced transport parameters are derived by combining an empirical relationship between the diffusive and total exchange flux of O_2 across the SWI with physical models of diffusive and nonlocal solute transport in sediments. The choice of O_2 as the enhanced transport tracer is dictated by the rapidly growing body of O_2 microprofile data and benthic chamber flux measurements. An added advantage is the high reactivity of O_2, which causes the benthic flux and profile of O_2 to rapidly adjust to changes in external forcings, for example, the deposition flux of organic matter. Thus, the proposed approach might also be suited to quantifying seasonal variations in enhanced transport intensity.

The effect of enhanced transport on sediment–water column exchanges is most pronounced in coastal marine environments, where the oxic zone tends to be very thin. Oxygen pore-water profiles therefore mainly contain information on enhanced transport properties close to the SWI, although irrigation could affect pore-water chemistry well below the oxic surface layer (e.g., Furukawa et al. 2000). In addition, the enhanced transport parameters of different chemical species might differ because of differences in diffusive properties and reactive length scales around macrofaunal burrows (e.g., Aller 2001; Koretsky et al. 2002).

In shallow-water permeable sediments, wave-induced pressure fluctuations cause advective solute transport (e.g., Huettel and Webster 2001), a mechanism not explicitly considered here. Frequently, these sediments are also inhabited by active populations of macrofauna; hence, several mechanisms can contribute simultaneously to enhanced pore-water transport (D'Andrea et al. 2002). In nearshore environments, the end-member transport models used here could thus no longer offer reliable ways to estimate benthic exchange fluxes. Furthermore, the simple interpretation of O_2 pore-water profiles, which assumes O_2 is only consumed (Eq. 5), is not valid when benthic photosynthesis becomes significant (e.g., Jahnke et al. 2000).

The above concerns point to the need for further work on enhanced transport in coastal sediments. In particular, efforts should focus on better constraining the uncertainties associated with the transfer of enhanced transport properties determined for O_2 to other chemical species and on developing more advanced models for the complex solute transport dynamics in nearshore sediments. Future studies could also integrate the predictive relationships of enhanced pore-water transport presented here in regional ocean studies, such as using GIS modeling tools (e.g., Schlüter et al. 2000). Such studies could then account for region-specific effects on sediment–water column exchanges related to, for instance, the bottom water oxygen distribution and organic matter deposition flux.

References

ALLER, R. C. 2001. Transport and reactions in the bioirrigated zone, p. 269–301. *In* B. P. Boudreau and B. B. Jørgensen [eds.], The benthic boundary layer. Oxford Univ. Press.

ARCHER, D., AND A. DEVOL. 1992. Benthic oxygen fluxes on the Washington shelf and slope: A comparison of in situ microelectrode and chamber flux measurements. Limnol. Oceanogr. **37:** 614–629.

———, J. L. MORFORD, AND S. R. EMERSON. 2002. A model of suboxic sedimentary diagenesis suitable for automatic running and gridded global domains. Glob. Biogeochem. Cycles **16:** 1288–1333.

BERG, P., N. RISGAARD-PETERSEN, AND S. RYSGAARD. 1998. Interpretation of measured concentration profiles in sediment pore water. Limnol. Oceanogr. **43:** 1500–1510.

———, S. RYSGAARD, P. FUNCH, AND M. K. SEJR. 2001. Effects of bioturbation on solutes and solids in marine sediments. Aquat. Microb. Ecol. **26:** 81–94.

BOUDREAU, B. P. 1984. On the equivalence of nonlocal and radial-diffusion models for porewater irrigation. J. Mar. Res. **42:** 731–735.

———. 1986*a*. Mathematics of tracer mixing in sediments: I. Spatially-dependent, diffusive mixing. Am. J. Sci. **286:** 161–198.

———. 1986*b*. Mathematics of tracer mixing in sediments: II. Nonlocal mixing and biological conveyor-belt phenomena. Am. J. Sci. **286:** 199–238.

———. 1994. Is burial velocity a master parameter for bioturbation? Geochim. Cosmochim. Acta **58:** 1243–1249.

———. 1997. Diagenetic models and their implementation. Springer.

———, AND D. IMBODEN. 1987. Mathematics of tracer mixing in sediments: III. The theory of nonlocal mixing within sediments. Am. J. Sci. **287:** 693–719.

———, AND B. B. JØRGENSEN. 2001. The benthic boundary layer. Oxford Univ. Press.

———, AND OTHERS. 2001. Permeable marine sediments: Overturning an old paradigm. EOS **82:** 133–136.

CAI, W.-J., AND C. E. REIMERS. 1995. Benthic oxygen flux, bottom water oxygen concentration and core top organic carbon content in the deep northeast Pacific Ocean. Deep-Sea Res. I **42:** 1681–1699.

CHRISTENSEN, J. P., A. H. DEVOL, AND W. M. SMETHIE. 1984. Bi-

ological enhancement of solute exchange between sediments and bottom water on the Washington continental shelf. Cont. Shelf Res. **3:** 9–23.

COLMAN, A. S., AND H. D. HOLLAND. 2000. The global diagenetic flux of phosphorus from marine sediments to the oceans: Redox sensitivity and the control of atmospheric oxygen levels, p. 53–75. *In* C. R. Glenn, L. Prévôt-Lucas, and J. Lucas [eds.], Marine authigenesis: From global to microbial. Society of Sedimentary Geology, SEPM Special Publication No. 64.

D'ANDREA, A. F., R. C. ALLER, AND G. R. LOPEZ. 2002. Organic matter flux and reactivity on a South Carolina sandflat: The impacts of porewater advection and macrobiological structures. Limnol. Oceanogr. **47:** 1056–1070.

DEVOL, A. H., AND J. P. CHRISTENSEN. 1993. Benthic fluxes and nitrogen cycling in sediments of the continental margin of eastern North Pacific. J. Mar. Res. **51:** 345–372.

EMERSON, S., R. JAHNKE, AND D. HEGGIE. 1984. Sediment–water exchange in shallow water estuarine sediments. J. Mar. Res. **42:** 709–730.

FERDELMAN, T. G., H. FOSSING, AND K. NEUMANN. 1999. Sulfate reduction in surface sediments of the southeast Atlantic continental margin between 15°38′S and 27°57′S (Angola and Namibia). Limnol. Oceanogr. **44:** 650–661.

FORSTER, S., R. N. GLUD, J. K. GUNDERSEN, AND M. HUETTEL. 1999. In situ study of bromide tracer and oxygen flux in coastal sediments. Estuar. Coast. Shelf Sci. **49:** 813–827.

FOSSING, H., T. G. FERDELMAN, AND P. BERG. 2000. Sulfate reduction and methane oxidation in continental margin sediments influenced by irrigation (South-East Atlantic off Namibia). Geochim. Cosmochim. Acta **64:** 897–910.

FURUKAWA, Y., S. BENTLEY, A. SHILLER, D. LAVOIE, AND P. VAN CAPPELLEN. 2000. The role of biologically-enhanced pore water transport in early diagenesis: An example from carbonate sediments in the vicinity of North Key Harbor, Dry Tortugas National Park, Florida. J. Mar. Res. **58:** 493–522.

GLUD, R. N., J. K. GUNDERSEN, AND B. B. JØRGENSEN. 1994. Diffusive and total oxygen uptake of deep-sea sediments in the eastern South Atlantic Ocean: In situ and laboratory measurements. Deep-Sea Res. I **41:** 1767–1788.

———, O. HOLBY, F. HOFFMANN, AND D. CANFIELD. 1998. Benthic mineralisation and exchange in Arctic sediments (Svalbard, Norway). Mar. Ecol. Prog. Ser. **173:** 237–251.

GOLDHABER, M. B., R. C. ALLER, J. K. COCHRAN, J. K. ROSENFELD, C. S. MARTENS, AND R. A. BERNER. 1977. Sulfate reduction diffusion and bioturbation in Long Island Sound sediments: Report of the FOAM group. Am. J. Sci. **277:** 193–237.

HAMMOND, D. E., H. J. SIMPSON, AND G. MATHIEU. 1977. Radon-222 distribution and transport across the sediment–water interface in the Hudson River estuary. J. Geophys. Res. **82:** 3913–3920.

HUETTEL, M., AND I. T. WEBSTER. 2001. Porewater flow in permeable sediments, p. 144–179. *In* B. P. Boudreau and B. B. Jørgensen [eds.], The benthic boundary layer. Oxford Univ. Press.

JAHNKE, R. A. 2001. Constraining organic matter cycling with benthic fluxes, p. 302–319. *In* B. P. Boudreau and B. B. Jørgensen [eds.], The benthic boundary layer. Oxford Univ. Press.

———, J. R. NELSON, R. L. MARINELLI, AND J. E. ECKMAN. 2000. Benthic flux of biogenic elements on the Southeastern US continental shelf: Influence of pore water advective transport and benthic microalgae. Cont. Shelf Res. **20:** 109–127.

JØRGENSEN, B. B., AND N. P. REVSBECH. 1985. Diffusive boundary layers and the oxygen uptake of sediments and detritus. Limnol. Oceanogr. **30:** 111–122.

KORETSKY, C. M., C. MEILE, AND P. VAN CAPPELLEN. 2002. Quantifying bioirrigation using ecological parameters: A stochastic approach. Geochem. Trans. **3:** 17–30.

LEVITUS, S., AND T. BOYER. 1994. World ocean atlas. NOAA Atlas NESDIS, U.S. Department of Commerce.

MARTIN, W. R., AND G. T. BANTA. 1992. The measurement of sediment irrigation rates: A comparison of the Br^- tracer and $^{222}Rn/^{226}Ra$ disequilibrium techniques. J. Mar. Res. **50:** 125–154.

———, AND F. L. SAYLES. 1994. Seafloor diagenetic fluxes, p. 143–163. *In* Board on Earth Sciences and Resources Commission on Geosciences, Environment, and Resources: National Resource Council [eds.], Material fluxes on the surface of the Earth. National Academy Press.

MATISOFF, G., AND X. WANG. 1998. Solute transport in sediments by freshwater infaunal bioirrigators. Limnol. Oceanogr. **43:** 1487–1499.

MCCAFFREY, R. J., AND OTHERS. 1980. The relation between pore water chemistry and benthic fluxes of nutrients and manganese in Narragansett Bay, Rhode Island. Limnol. Oceanogr. **25:** 31–44.

MEILE, C., C. KORETSKY, AND P. VAN CAPPELLEN. 2001. Quantifying bioirrigation in aquatic sediments: An inverse modeling approach. Limnol. Oceanogr. **46:** 164–177.

MIDDELBURG, J. J., K. SOETAERT, AND P. M. HERMAN. 1997. Empirical relationships for use in global diagenetic models. Deep-Sea Res. I **44:** 327–344.

NATIONAL GEOPHYSICAL DATA CENTER. 1988. Digital relief of the surface of the Earth (ETOP05), Data Announcement 88-MGG-02. NOAA.

REIMERS, C. E., AND K. L. J. SMITH. 1986. Reconciling measured and predicted fluxes of oxygen across the deep sea sediment–water interface. Limnol. Oceanogr. **31:** 305–318.

———, R. A. JAHNKE, AND D. C. MCCORKLE. 1992. Carbon fluxes and burial rates over the continental slope and rise off Central California with implications for the global carbon cycle. Glob. Biogeochem. Cycles **6:** 199–224.

———, ———, AND L. THOMSEN. 2001. In situ sampling in the benthic boundary layer, p. 245–268. *In* B. P. Boudreau and B. B. Jørgensen [eds.], The benthic boundary layer. Oxford Univ. Press.

RØY, H., M. HUETTEL, AND B. B. JØRGENSEN. 2002. The role of small-scale topography for oxygen flux across the diffusive boundary layer. Limnol. Oceanogr. **47:** 837–847.

SAYLES, F. L., W. R. MARTIN, AND W. G. DEUSER. 1994. Response of benthic oxygen demand to particulate organic carbon supply in the deep sea near Bermuda. Nature **371:** 686–689.

SCHLÜTER, M., E. J. SAUTER, A. SCHÄFER, AND W. RITZRAU. 2000. Spatial budget of organic carbon flux to the seafloor of the northern North Atlantic (60°N–80°N). Glob. Biogeochem. Cycles **14:** 329–340.

SMETHIE, W. M. J., C. A. NITTROUER, AND R. F. L. SELF. 1981. The use of radon-222 as a tracer of sediment irrigation and mixing on the Washington continental shelf. Mar. Geol. **42:** 173–200.

SOETAERT, K., P. M. J. HERMAN, AND J. J. MIDDELBURG. 1996*a*. Dynamic response of deep-sea sediments to seasonal variations: A model. Limnol. Oceanogr. **41:** 1651–1668.

———, ———, AND ———. 1996*b*. A model of early diagenetic processes from the shelf to abyssal depths. Geochim. Cosmochim. Acta **60:** 1019–1040.

———, J. J. MIDDELBURG, P. M. J. HERMAN, AND K. BUIS. 2000. On the coupling of benthic and pelagic biogeochemical models. Earth Sci. Rev. **51:** 173–201.

TROMP, T. K., P. VAN CAPPELLEN, AND R. M. KEY. 1995. A global model for the early diagenesis of organic carbon and organic phosphorus in marine sediments. Geochim. Cosmochim. Acta **59:** 1259–1284.

VAN CAPPELLEN, P., AND Y. WANG. 1996. Cycling of iron and manganese in surface sediments: A general theory for the coupled

transport and reaction of carbon, oxygen, nitrogen, sulfur, iron and manganese. Am. J. Sci. **296:** 197–243.

VANDERBORGHT, J. P., R. WOLLAST, AND G. BILLEN. 1977. Kinetic models of diagenesis in disturbed sediments. Part 1. Mass transfer properties and silica diagenesis. Limnol. Oceanogr. **22:** 787–793.

WANG, Y., AND P. VAN CAPPELLEN. 1996. A multicomponent reactive transport model of early diagenesis: Application to redox cycling in coastal marine sediments. Geochim. Cosmochim. Acta **60:** 2993–3014.

WENZHÖFER, F., AND R. GLUD. 2002. Benthic carbon mineralization in the Atlantic: A synthesis based on in situ data from the last decade. Deep-Sea Res. I. **49:** 1255–1279.

WIJSMAN, J. 2000. Early diagenetic processes in Northwestern Black Sea sediments. Ph.D. thesis, Groningen Univ., The Netherlands. Available at http://www.ub.rug.nl/eldoc/dis/science/j.w.m.wijsman/.

ZIEBIS, W., M. HUETTEL, AND S. FORSTER. 1996. Impact of biogenic sediment topography on oxygen fluxes in permeable seabeds. Mar. Ecol. Prog. Ser. **140:** 227–237.

Received: 22 March 2002
Accepted: 21 October 2002
Amended: 29 October 2002